


Computation of the change in length of a braided device when deployed in realistic vessel models

Hector Fernandez¹  · Juan M. Macho² · Jordi Blasco² · Luis San Roman² · Werner Mailaender³ · Luis Serra¹ · Ignacio Larrabide⁴

Received: 18 January 2015 / Accepted: 28 May 2015
© CARS 2015

Abstract

Purpose An important issue in the deployment of braided stents, such as flow diverters, is the change in length, also known as foreshortening, underwent by the device when is released from the catheter into a blood vessel. The position of the distal end is controlled by the interventionist, but knowing a priori the position of the proximal end of the device is not trivial. In this work, we assess and validate a novel computer method to predict the length that a braided stent will adopt inside a silicon model of an anatomically accurate vessel.

Methods Three-dimensional rotational angiography images of aneurysmatic patients were used to generate surface models of the vessels (3D meshes) and then create accurate silicon models from them. A braided stent was deployed into each silicon model to measure its length. The same stents deployed on the silicon models were virtually deployed on the 3D meshes using the method being evaluated.

Results The method was applied to five stent placements on three different silicon models. The length adopted by the real braided device in the silicon models varies between 15 and 30 % from the stent length specified by the manufacturer. The final length predicted by the method was within the estimated error of the measured real stent length.

Conclusions The method provides, in a few seconds, the length of a braided stent deployed inside a vessel, showing an accurate estimation of the final length for the cases studied. This technique could provide useful information for planning the intervention and improve endovascular treatment of intracranial aneurysms in the future.

Keywords Flow diverter · Braided stents · Length change prediction · Intracranial aneurysms

Introduction

An increasing number of braided stents are being used in endovascular treatment of intracranial aneurysms (IAs) [7, 22, 24]. These devices have the advantage of being highly maneuverable, allowing the interventional neuroradiologist to reach distal regions within the intracranial vasculature. One treatment that became popular in the past few years is the use of flow diverters (FDs) for aneurysm occlusion. These are braided devices with a dense mesh of interwoven wires, having 24 wires and more. FDs are used to change hemodynamic conditions inside of the aneurysm, redirecting blood flow away from the aneurysm into the parent vessel [12], thus promoting controlled thrombosis inside the aneurysm sac and restoring normal blood flow [18].

One of the main technical problems of FDs and, by extension, of any braided device is that it is hard to predict the final length of the device inside the vessel, which results in a considerable foreshortening after deployment. This foreshortening depends on the patient's vasculature [4, 8]. The positioning of the device can be critical if it happens to occlude adjacent arteries, if the proximal ends lay on high curvature regions or if there is risk of device migration after

✉ Hector Fernandez
hector.fernandez@galgomedical.com

Ignacio Larrabide
larrabide@exa.unicen.edu.ar;
ignacio.larrabide@galgomedical.com

¹ Galgo Medical S.L., Barcelona, Spain

² Hospital Clinic Provincial de Barcelona, Barcelona, Spain

³ Acandis GmbH, Pforzheim, Germany

⁴ Pladema, CONICET, UNICEN, Tandil, Argentina

deployment [14,21]. Migration of the device can happen for several reasons, among them: a loose apposition on the vessel wall or due to squeezing forces at the edges of the device that make it slip backwards. Moreover, shortening of braided stents after deployment has been observed if the device is stretched during the intervention [5]. The final length can also affect the hemodynamic performance of the FD [17].

Having an accurate prediction of the length that the FD will adopt before its placement can be helpful in planning a clinical intervention and assess the use of the stretching or packaging on the device with respect to the standard release inside the vessel.

Different computational methods have been proposed in the literature to model endovascular devices. The method presented by Appanaboyina et al. [1] focus on the generation of a geometrical representation of a FD for the simulation of post-treatment hemodynamics. More recent work of Larrabide et al. [11] and Peach et al. [19] has focused on the representation of the devices and its validation with finite element mechanical models [3] and its use in computational fluid mechanics [2]. The work of Ma et al. [15] presents a methodology for the mechanical simulation of FDs that applies finite element analysis to generate a detailed model of the device mechanics and its individual threads. A similar approach was previously applied to optimize the foreshortening undergone by a FD during unconfined free release from the catheter [6].

None of the methods mentioned above can predict the foreshortening of a FD after insertion in the vasculature of a real patient in a way that is both fast and accurate. A method for the computation of such change in length has been recently proposed that rapidly computes the length of a braided device when released inside a vessel [10]. In this work, we present a validation of this method in silicon models.

Methodology

This section describes the technical procedure to determine the final length of a FD before its placement inside a vascular structure. The proposed algorithm allows determining the proximal end point provided the distal end point of the FD. It is based on the analysis of the foreshortening of the FD due to the local vessel morphology. This methodology requires a function that calculates the relation between the length change of the FD and the local vascular morphology.

Braided device foreshortening algorithm

The braided device foreshortening (BDF) algorithm predicts the foreshortening of a FD, see [10]. The method is based on the analysis of the local morphology at the region where the device is released.

A 3D mesh of the vessel is needed for the application of BDF. This 3D mesh consists on a computational model of the lumen from which the local morphology of the vessel is characterized. This local morphology is associated with the vessel cross section (perpendicular to its centerline), and it is described by the diameter of the maximum inscribed sphere, perimeter of the vessel and cross-sectional area.

The centerline of these 3D meshes and the local morphology descriptors along the centerline were obtained using the open source tool VMTK [20,23]. The centerline was divided into segments sufficiently small such that local morphological variables were almost constant along each segment.

The morphology descriptors of the vessel at each segment and a length change function (LCF) for each device are the input of the BDF algorithm. We define the nominal configuration of the FD as the length and diameter adopted by the FD when is released free outside the vessel. Once the user selects the distal end point, the method is then applied to each segment toward the proximal end of the centerline and calculates the amount of nominal FD length needed to cover each segment [10]. The method ends at the point of the centerline where the total sum of covered segments is equal to the nominal length of the FD.

The final FD length is the distance between the starting distal point and the final proximal point calculated by BDF along the centerline. If we consider that a FD has a cylindrical geometry and that its structure tends to maintain this configuration when released, the FD is then approximated by a tube whose local radius is the maximum inscribed sphere at each segment of the centerline.

The average time required for the execution of this algorithm on a standard computer configuration (Intel i7, 2.20GHzx8, 8GB, with no parallelization) is in the range of 2–3 s, which is considerably faster than similar methods based on finite element analysis, with computational times in the order of hours [6].

Length change function

The LCF is used to compute the foreshortening of a section of the device. A FD is a cylindrical tube made of interlaced braids arranged in a helical shape that maintains its interwoven pattern after deformation. Figure 1 shows a schematic draw of a FD, where braiding angle, diameter and strut length are shown. A strut of a FD is the line enclosed between adjacent crossings of the interlaced wires. The number of struts in a FD is constant and depends on the wire turns per unit length.

Because the length of a wire is constant at any position of the device, the foreshortening underwent by the stent when released is related to the diameter through the helix equation. This can be easily applied to a constant radial deformation

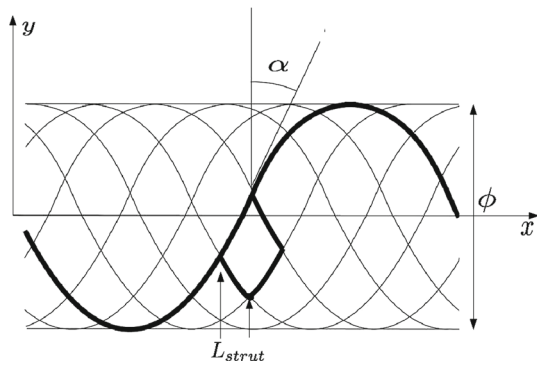


Fig. 1 Detail of a FD, the interlaced threads are arranged in a sinusoidal pattern along the stent length. The angle between threads, α , determines the diameter of the stent, ϕ , and the stent length by changing the projection of L_{strut} along its x axis

along the device length to calculate the foreshortening for different diameter configurations.

The LCF is calculated for deployment conditions where the device is not affected by pushing or pulling the catheter, and thus, the maximum diameter available for the FD expansion corresponds to the diameter at the nominal position [10]. This assumption can limit the method's accuracy, and it has not been considered on this study. Such effects are currently under study.

The LCF can also be obtained experimentally, by measuring the local shape parameters of a FD when deployed on tubes of different shapes and sizes. This would provide a function of the length versus the diameter of the device, and this can be comparable to the FD lengths at different diameters provided by the manufacturing companies.

Materials

The validation of the proposed method was done on FDs. Three-dimensional RA images from three patients were used, from which 3D meshes were obtained by applying a marching cubes algorithm with a threshold of the 10% of the maximum pixel value [13]. The meshes obtained were used to generate 3D silicon models with a 3D printer to deploy FDs inside. The data used for the validation were as follows:

1. a set of photographs of the silicon models with the FDs released inside.
2. 3DRA images of the silicon models with the FDs released inside.

Figure 2 shows the 3D meshes of the three cases. The anatomical models were provided by Acandis GmbH (Pforzheim, Germany). Model P1 was obtained using an Integriss™ Allura System (Philips Healthcare, Best, Netherlands) with a spatial resolution of $0.08 \times 0.08 \times 0.08$ mm. Models

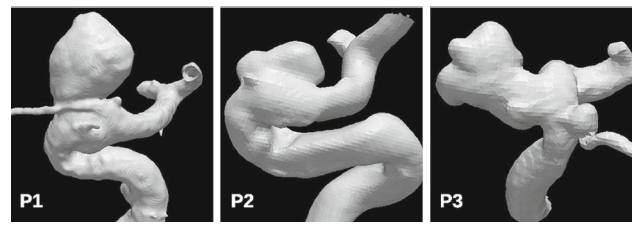


Fig. 2 3D meshes used to evaluate the BDF algorithm. The meshes were created with a marching cubes algorithm from 3DRA images of real patients. Aneurysms from P1 and P2 are placed at the internal carotid artery close to the middle cerebral artery bifurcation. P3 is also located at the internal carotid artery with a small aneurysm at the base of the ophthalmic artery

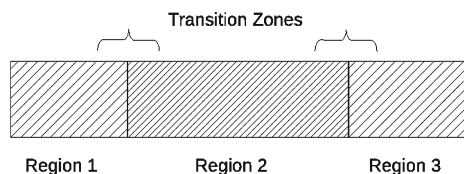
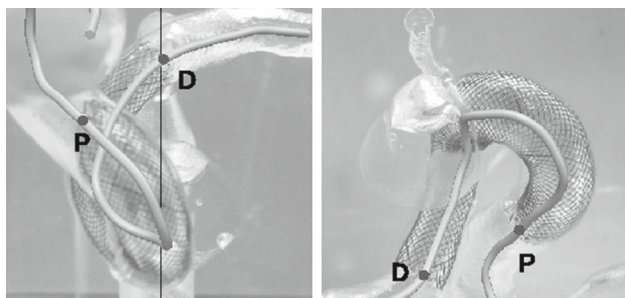
P2 and P3 were obtained using an AXIOM Artis (Siemens Medical Solutions, Erlangen, Germany) with a spatial resolution of $0.362 \times 0.362 \times 0.362$ mm. All cases correspond to saccular aneurysms at the internal carotid artery close to the bifurcation. Patient P3 shows a second small aneurysm at the ophthalmic artery bifurcation, contralateral to the larger one.

Two FDs designed by Acandis GmbH have been used, Derivo 4.0×25 (D4.0 \times 25) and Derivo 4.5×20 (D4.5 \times 20). The FDs were selected following the criteria usually followed by clinicians when selecting a FD for a specific patient. The FD design is detailed on Table 1 for the nominal configuration. Both FDs are manufactured with three different regions. The central region presents more wire turns per unit length, thus showing a denser mesh with more struts per unit length. This is done with the purpose of further decreasing the inflow into the aneurysm, and this part of the FD should be placed to cover the aneurysm neck region. The transition between regions with different mesh densities is smooth and can vary between different stents of the same diameter and length. Figure 3 shows schematically the structure of Derivo. The central region at the nominal position of D4.0 \times 25 occupies $(52 \pm 3)\%$ of the FD length. The central region at the nominal position of D4.5 \times 20 occupies $(43 \pm 3)\%$ of the FD length. The transition zone can be slightly different between FDs within the safety margins established by the manufacturing process. This variability occurs because of the transition of the braiding angle between neighboring regions, which can vary the number of struts on each region. The variability of the transition zone is then modeled with the BDF by defining a maximum and minimum length change (Table 1).

Five cases were used to validate the algorithm. An interventional neuroradiologist experienced in FD treatment deployed the FDs into the three silicon models P1, P2 and P3. A specialist from the manufacturing company also released the same two FDs inside P2 and P3. D4.0 \times 25 was released into model P1, and D4.5 \times 20 was released into models P2 and P3.

Table 1 Derivo FD design parameters, namely nominal diameter, nominal length, ϕ and number of struts at each region

Stent	Nominal ϕ (mm)	Nominal length (mm)	Region 1 min–max	Region 2 min–max	Region 3 min–max
D4.5 × 20	4.66	14	9–17	33–44	11–17
D4.0 × 25	4.16	17	9–17	56–75	11–17

**Fig. 3** Schematic representation of a Derivo FD, which presents three different mesh densities. The central region (more dense) is designed to be placed at the region of the vessel affected by the aneurysm. Due to the manufacturing process, the transition between regions is smooth, leading to a zone on which the braiding angle smoothly ranges between the braiding angles of the two neighboring regions**Fig. 4** Photographs of the 3D silicon model of P2 for two different points of view. The manual registration of the 3D mesh to the photographs allows superimpose the centerline. Points *D* and *P* refer to the estimated distal and proximal ends of the released device. The distance between both points determines the length of the FD deployed on the silicon models

The length of the deployed FD in the transparent silicon models was estimated using photographs taken from several points of views. Using the photographs as image background, the corresponding 3D mesh was manually oriented to visually match them. Distal and proximal points of the FD were identified on the photographs and then marked on the corresponding 3D centerline of the surface mesh (Fig. 4). On average, three different viewpoints were used for each case.

The length measured from the photographs of the real deployed stents was compared to the predicted length of the FD calculated with our method. For cases P2 and P3, an additional 3DRA was performed with the released FD inserted by the neuroradiologist. This allowed performing a true 3D comparison between the deployed stent and the prediction of BDF and validating the measurement method used on the photographs.

Results and discussion

Figure 5 shows the results for models P1, P2 and P3 treated by the neuroradiologist compared to the BDF prediction. The results for all treated cases are listed in Table 2. The label sub-figure PXY refers to PX as the patient (P1, P2 and P3) and Y to the interventionist that released the FD. Table 2 shows the real, the predicted minimum and predicted maximum FD lengths for five cases. The maximum and minimum change in length for the FD ranges from 50 (P11) to 94% (P21) of the FD nominal length (Table 1). These values are relatively higher than those reported on FD for releasing from the catheter to the nominal position [6].

The proposed method assumes a normal delivery of the device inside the vessel and does not account for packing by the interventionist during the FD deployment. The silicon model is rigid, and therefore, the FD does not impose any radial deformation on the vessel wall. This might not hold when treating real patients. Still, the vessel radial deformation is much smaller for nitinol FDs, such as Derivo, than for cobalt-chromium alloy FDs, whose radial force is considerably higher [16].

It can be noticed from Fig. 5 and Table 2 that the BDF prediction of the maximum length shows the best fit. The reason can be that, for a FD of a given diameter and length, the transition between regions is smooth, and the braided angle gradually changes from one region to the next, thus changing the density of the mesh and the number of struts. The contribution to the foreshortening is higher for regions with more struts independently of the region they belong to. Those parts (close to the center) from the external regions that show a higher density compensate the lower density at the edges of the central region. As the contribution to the foreshortening of the denser regions is higher, the result adapts better to the maximum length change. Further studies with more cases could help on a better understanding of this behavior.

Both maximum and minimum predicted FD lengths are shown in Fig. 5, according to the variability at the transition regions of the device. The red, green and blue colors correspond to the regions with different mesh densities of the Derivo. Since there is no visual indication on the device, it is difficult to the naked eye of the interventionist to estimate where the different regions start and end. The proposed method provides a visual guide to the interventionist for placing the central region under the aneurysm neck.

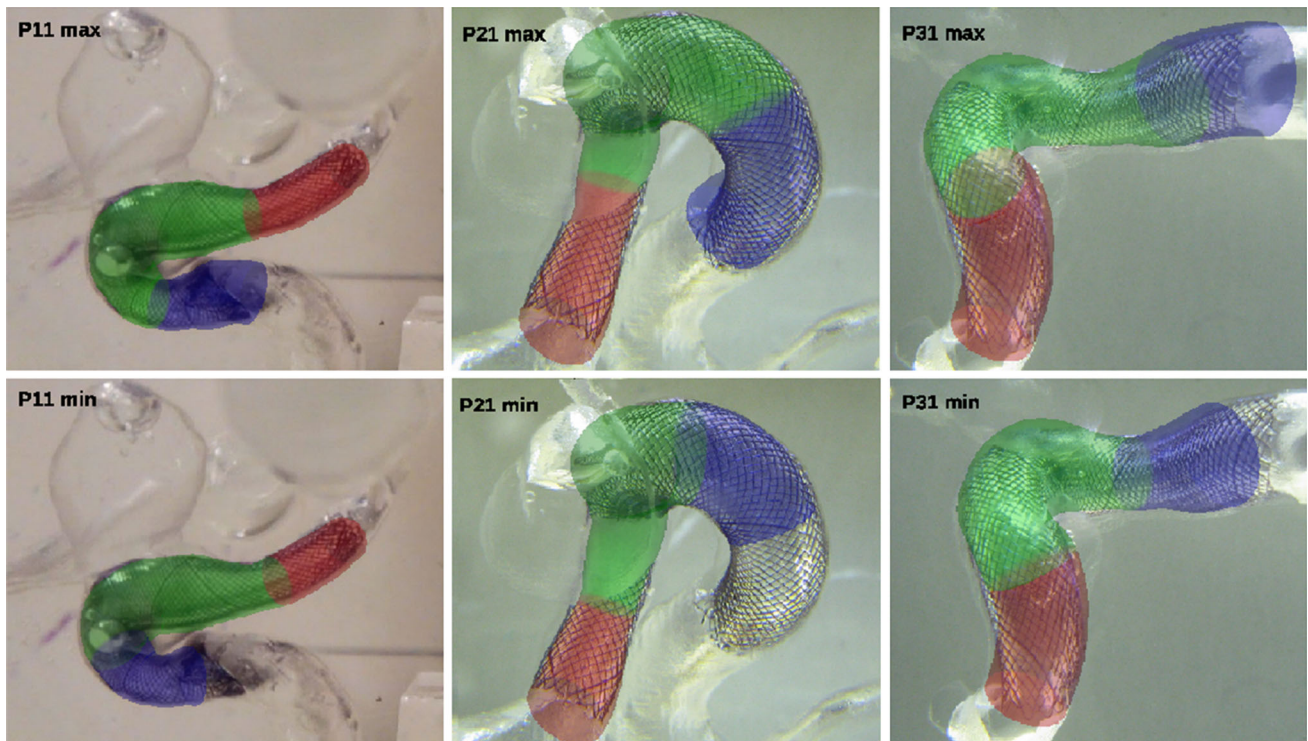


Fig. 5 Maximum (*top*) and minimum (*bottom*) FD predicted length compared with photographs of the real cases for those deployed by the interventional neuroradiologist. *Color* indicates regions with different

mesh densities. *Green region*, which presents the denser mesh, should be placed below the aneurysm neck

Table 2 The columns in the table present the case number, the FD used in that case, the real length of the device measured from three photographs for each case (showing mean and SD) the length simulated

by the studied method (both, minimum and maximum) and the mean vessel diameter in the region occupied by the FD

Case	Stent	Real length (mean \pm SD) (mm)	Simulated length (min–max) (mm)	Mean vessel ϕ (mean \pm SD) (mm)
P11	D4.0 \times 25	26.054 \pm 1.289	22.745–26.163	3.339 \pm 0.589
P21	D4.5 \times 20	27.389 \pm 0.849	21.547–26.874	3.697 \pm 0.501
P31	D4.5 \times 20	26.616 \pm 0.751	22.271–26.201	3.771 \pm 0.370
P22	D4.5 \times 20	26.179 \pm 0.122	22.516–27.116	3.634 \pm 0.460
P32	D4.5 \times 20	26.213 \pm 1.043	22.500–26.662	3.715 \pm 0.348

Figure 6 shows the lengths adopted by the FDs at different diameters, using the data provided by the manufacturer. Notice that for diameter changes from 4 to 3 mm, the associated length goes from 25 to 40 mm. The measured FD length on the silicon models is also shown on the figure. For the same mean vessel diameter, an irregular tubular structure, like the internal carotid artery, can lead to FD lengths far from the data provided by the manufacturer. As the mean diameter of the vessel decreases with respect to the FD nominal diameter, the difference between the measured and expected length increases, leading to unpredictable situations during the intervention.

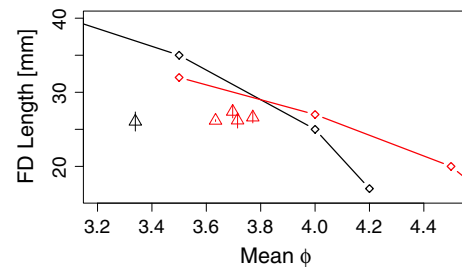


Fig. 6 Real FD measured length (*triangle*) with *error bars* and the manufacturer specifications (*diamond*) against the vessel mean diameter for D4.0 \times 25 (*black*) and D4.5 \times 20 (*red*). The *lines* connecting the manufacturer values are a guide for intermediate diameter values

Figure 7 shows the measured, maximum and minimum predicted FD lengths versus the mean diameter of the vessel along the region occupied by the FD. From Table 2, we observe that the range of the mean vessel diameter is on the order of the SD of each case. Therefore, it is not possible to infer a function of FD length dependent on this parameter. The maximum difference between measured and maximum predicted lengths is approximately 3% for case P22. Comparing the FD lengths from Figs. 6 and 7 for the same vessel diameter, differences of 15–30% are obtained with respect to lengths provided by the manufacturer.

Previous works have assessed the length change for a constant radial deformation along the stent length [6,9,15]. In this work, the assessment was done on anatomically accu-

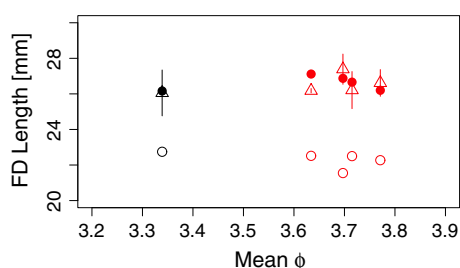


Fig. 7 Real FD measured length (triangle) with error bars and predicted maximum length (filled circle) and minimum length (open circle) plotted versus vessel mean diameter for D4.0 × 25 (black) and D4.5 × 20 (red) ϕ

rate vessel models. Figure 8 shows the maximum predicted length of D4.5 × 20 for the cases P21 and P31 compared with the 3DRA of the FD released inside the silicon model. The vessel is shown in red, while the predicted FD is shown in green. The real FD radiopaque threads (markers) are also visible in semitransparent blue. It can be observed that the distal and proximal end points of the device show a good match between the real and predicted case. Also, the surface of the real FD nicely follows the surface of the predicted FD. The predicted FD fits the adaptation of the FD to the aneurysm neck, except at the distal zone on case P21, where the real stent herniates into the aneurysm sac. Further studies have to be carried out to improve the adaptation of the stent to the vessel wall. For a first approximation, the proposed method provides a simple way to estimate the final length of the FD and helps inferring regions that are in contact with the vessel wall with small computational cost [15].

Conclusions

A method to calculate the length of a FD inside a vessel has been assessed in this work. The method is based on the use of a Length Change Function and a representation of the vessel with appropriate local morphology information. The computational time of the algorithm is in the order of 2–3 s, thus being a promising technique for helping clini-

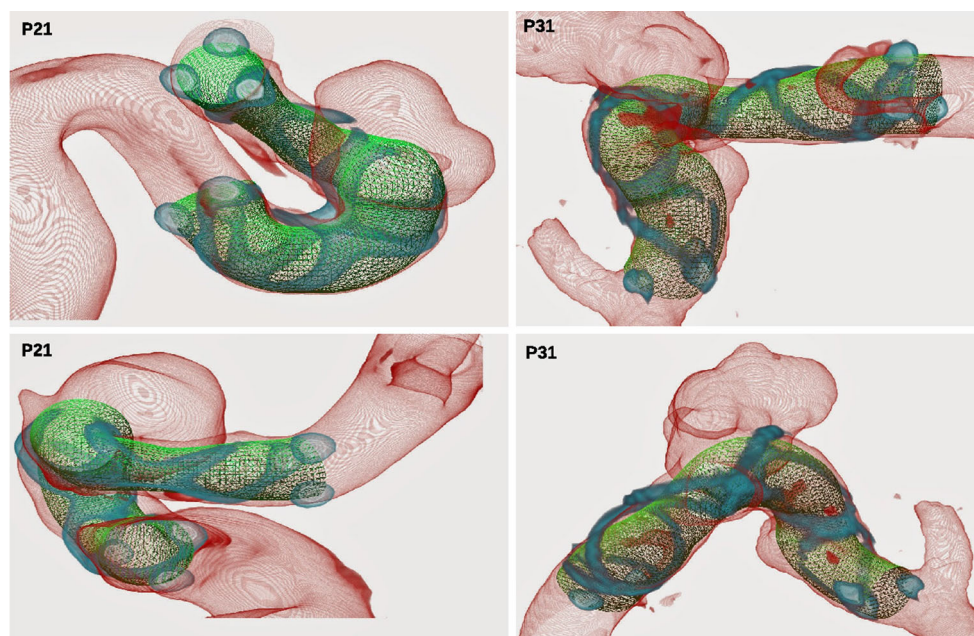


Fig. 8 Comparison of a 3DRA volume rendering of the silicon models with the FD deployed inside against the predicted FD maximum length change for cases P21 (left) and P31 (right). In both cases, the FD used was a D4.5 × 20 deployed by the interventional neuroradiologist. The

blue spots at the end of the FD correspond to the radiopaque markers. The predicted FD is shown as a green wireframe mesh inside the vessel

cal decisions in real time. A validation of the method has been presented for saccular aneurysms comparing the real and predicted FD lengths. A 3D comparison of deployed and predicted results is also shown in two cases, with an accurate matching between them. The real and predicted lengths are 30–15% lower than the lengths provided by the manufacturer. Further clinical validation with more cases is currently under development. Results are promising, indicating that this technique could provide useful information for improved endovascular treatment of IAs in the future.

Conflict of interest H. Fernandez, L. Serra and I. Larrabide are stockholders in Galgo Medical S.L.; W. Mailaender is employed by Acandis GmbH.

References

1. Appanaboyina S, Mut F, Löhner R, Putman CM, Cebal JR (2009) Simulation of intracranial aneurysm stenting: techniques and challenges. *Comput Methods Appl Mech Eng* 198(45):3567–3582
2. Bernardini A, Larrabide I, Morales HG, Pennati G, Petrini L, Cito S, Frangi AF (2011a) Influence of different computational approaches for stent deployment on cerebral aneurysm haemodynamics. *Interface Focus* 1(3):338–348
3. Bernardini A, Larrabide I, Petrini L, Pennati G, Flore E, Kim M, Frangi AF (2011b) Deployment of self-expandable stents in aneurysmatic cerebral vessels: comparison of different computational approaches for interventional planning. *Comput Methods Biomech Biomed Eng* 15(3):303–311
4. Chalouhi N, Satti S, Tjoumakaris S, Dumont A, Gonzalez L, Rosenwasser R, Jabbour P (2013a) Delayed migration of a pipeline embolization device. *Neurosurgery* 72(2 Suppl Operative):229–234
5. Chalouhi N, Tjoumakaris S, Gonzalez L, Hasan D, Pema P, Gould G, Rosenwasser R, Jabbour P (2013b) Spontaneous delayed migration/shortening of the pipeline embolization device: report of 5 cases. *AJNR* 34:2326–2330
6. De Beule M, Van Cauter S, Mortier P, Van Loo D, Van Impe R, Verdonck P, Verheghe B (2009) Virtual optimization of self-expandable braided wire stents. *Med Eng Phys* 31(4):448–453
7. Golitz P, Struffert T, Rosch J, Ganslandt O, Knossalla F, Doerfler A (2015) Cerebral aneurysm treatment using flow-diverting stents: in vivo visualization of flow alterations by parametric colour coding to predict aneurysmal occlusion: preliminary results. *Eur radiol* 25(2):428–435
8. Hauck E, Natarajan S, Langer D, Hopkins L, Siddiqui A, Levy EI (2010) Retrograde trans-posterior communicating artery snare-assisted rescue of lost access to a foreshortened pipeline embolization device: complication management. *Neurosurgery* 67(2 Suppl Operative):495–502
9. Jedwab MR, Clerc CO (1993) A study of the geometrical and mechanical properties of a self-expanding metallic stent-theory and experiment. *J Appl Biomater* 4(1):77–85
10. Larrabide I (2014) Procedimiento para la determinación de la longitud final de stents antes de su colocación. *Oficina Española de Patentes y Marcas (ES2459244 A1):P201331,605*
11. Larrabide I, Kim M, Augsburg L, Villa-Uriol MC, Rüfenacht DA, Frangi AF (2012) Fast virtual deployment of self-expandable stents: method and in vitro evaluation for intracranial aneurysmal stenting. *Med Image Anal* 16(3):721–730
12. Levitt MR, McGah PM, Aliseda A, Mourad P, Nerva J, Vaidya SS, Morton R, Ghodke B, Kim LJ (2014) Cerebral aneurysms treated with flow-diverting stents: computational models with intravascular blood flow measurements. *Am J Neuroradiol* 35(1):143–148
13. Lorensen WE, Cline HE, Company GE (1987) Marching cubes: a high resolution 3D surface construction algorithm. *Comput Graph (ACM)* 21(4):163–169
14. Lubicz B, Collignon L, Raphaeli G, Pruvo JP, Bruneau M, De Witte O, Leclerc X (2010) Flow-diverter stent for the endovascular treatment of intracranial aneurysms: a prospective study in 29 patients with 34 aneurysms. *Stroke* 41(10):2247–2253
15. Ma D, Dargush GF, Natarajan SK, Levy EI, Siddiqui AH, Meng H (2012) Computer modeling of deployment and mechanical expansion of neurovascular flow diverter in patient-specific intracranial aneurysms. *J Biomech* 45:1–8
16. Material Property Data (1990) <http://www.matweb.com>. Accessed 9 Feb 2015
17. Mut F, Cebal JR (2012) Effects of flow-diverting device oversizing on hemodynamics alteration in cerebral aneurysms. *Am J Neuroradiol* 33(10):2010–2016
18. Nelson PK, Lylyk P, Szikora I, Wetzel SG, Wanke I, Fiorella D (2011) The pipeline embolization device for the intracranial treatment of aneurysms trial. *Am J Neuroradiol* 32(1):34–40
19. Peach TW, Ngoepe M, Spranger K, Ventikos Y (2014) Personalizing flow-diverter intervention for cerebral aneurysms: from computational hemodynamics to biochemical modeling. *Int J Numer Meth Biomed Eng* 30:1387–1407
20. Piccinelli M, Veneziani A, Steinman DA, Remuzzi A, Antiga L (2009) A framework for geometric analysis of vascular structures: application to cerebral aneurysms. *IEEE Trans Med Imaging* 28(8):1141–1155
21. Rouchaud A, Leclerc O, Benayoun Y, Saleme S, Camilleri Y, D'Argento F, Boncoeur MP, Robert PY, Mounayer C (2015) Visual outcomes with flow-diverter stents covering the ophthalmic artery for treatment of internal carotid artery aneurysms. *AJNR Am J Neuroradiol* 36(2):330–336
22. Sadasivan C, Cesar L, Seong J, Rakian A, Hao Q, Tio FO, Wakhloo AK, Lieber BB (2009) An original flow diversion device for the treatment of intracranial aneurysms: evaluation in the rabbit elastase-induced model. *Stroke* 40(3):952–958
23. The Vascular Modelling Toolkit (VMTK) (2000) <http://www.vmtk.com>. Accessed 9 Feb 2015
24. Wong GKC, Lau JCY, Poon WS (2011) Flow diverters for treatment of intracranial aneurysms: current status and ongoing clinical trials. *J Clin Neurosci* 18(6):737–740